

Tau mediated coupling between Pol III synthesis and DnaB helicase unwinding helps maintain genomic stability

Malisha U. Welikala¹, Lauren, J. Butterworth¹, Megan S. Behrmann^{1,†}, and Michael A. Trakselis^{1*}

¹Department of Chemistry and Biochemistry, Baylor University, Waco, Texas, 76798-7348, USA

[†]Current Address: National Cancer Institute, Bethesda, MD, 20814, USA.

*To whom correspondence should be addressed: *Michael A. Trakselis, One Bear Place #97348, Waco, TX 76798-7348. Tel 254-710-2581; Email: michael_trakselis@baylor.edu

Author ORCIDs

Malisha U. Welikala ORCID: 0000-0001-6335-4509

Lauren J. Butterworth ORCID: 0000-0002-9410-2926

Megan S. Behrmann ORCID: 0000-0001-6788-9228

Michael A. Trakselis ORCID: 0000-0001-7054-8475

Keywords

coupling, decoupling, Tau, clamp loader, DNA helicase, unwinding, DNA replication, genomic instability

Abbreviations

Isopropyl β - d-1-thiogalactopyranoside (IPTG), clamp loader complex (CLC), single stranded DNA (ssDNA), triphenyltetrazolium chloride (TTC), 4',6-diamidino-2-phenylindole (DAPI), mitomycin C (MMC), green fluorescent protein (GFP), fluorescence-activated cell sorting (FACS), propidium iodide (PI)

Abstract

The τ -subunit of the clamp loader complex (CLC) physically interacts with both the DnaB helicase and the polymerase III (Pol III) core α -subunit through Domains IV and V, respectively. This interaction is proposed to help maintain rapid and efficient DNA synthesis rates with high genomic fidelity and plasticity, facilitating enzymatic coupling within the replisome. To test this hypothesis, CRISPR-Cas9 editing was used to create site-directed genomic mutations within the *dnaX* gene at the C-terminus of τ predicted to interact with the α -subunit of Pol III. Perturbation of the α - τ binding interaction *in vivo* resulted in cellular and genomic stress markers that included reduced growth rates, fitness, and viabilities. Specifically, *dnaX:mut* strains showed increased cell filamentation, mutagenesis frequencies, and activated SOS. *In situ* fluorescence flow cytometry and microscopy quantified large increases in the amount of single-stranded DNA (ssDNA) gaps present. Removal of the C-terminus of τ (I618X) still maintained its interactions with DnaB and stimulated unwinding but lost its interaction with Pol III, resulting in significantly reduced rolling circle DNA synthesis. Intriguingly, *dnaX:L635P/D636G* had the largest induction of SOS, high mutagenesis, and the most prominent ssDNA gaps, which can be explained by an impaired ability to regulate the unwinding speed of DnaB resulting in a faster rate of *in vitro* rolling circle DNA replication, inducing replisome decoupling. Therefore, τ stimulated DnaB unwinding and physical coupling with Pol III acts to enforce replisome plasticity to maintain an efficient rate of synthesis and prevent genomic instability.

Introduction

DNA replication in *Escherichia coli* has been well studied and shown to consist of a minimal replisome composed of at least 13 proteins that function together to ensure faithful and accurate replication of DNA (1). The main replicative helicase, DnaB, translocates in the 5' – 3' direction and unwinds double stranded DNA by encircling the lagging strand and sterically excluding the leading strand (2). The polymerase III (Pol III) holoenzyme consists of the core (α , ϵ , and θ subunits), which synthesize nascent DNA leading and lagging strands, a β clamp that interacts with Pol III to increase the processivity, and the clamp-loader complex (CLC) to load the β clamp (3). The CLC plays an important role as the central organizer of the replisome, coordinating clamp loading, coupling unwinding and synthesis, and maintaining equal rates for leading and lagging strand synthesis (4, 5).

Recent advances in single molecule technology both *in vitro* and *in vivo* have shown that the bacterial replisome is surprisingly dynamic with frequent exchanges of polymerases and accessory subunits in a concentration dependent manner, while the helicase remains a stable hub for the assembly of the rest of the replisome proteins (6-8). There is a dichotomy within the replisome between a more stable helicase complex as an anchor for unwinding and the more stochastic behavior of Pol III required for the discontinuous synthesis of Okazaki fragments or traversing challenging regions for synthesis (9). Therefore, a balance in maintaining continuity or coupling of the DNA unwinding and synthesis processes despite their differential dynamic equilibria processes must be maintained, highlighting significant variability and heterogeneity in replisomes (10). In the *E. coli* replisome, this continuity is thought to be maintained through a physical link between the polymerase and helicase provided by the τ -subunit of the CLC that helps regulate replication speed (Fig. 1A) (11).

The *dnaX* gene encodes for both τ and γ subunits; however, γ is a truncated form of τ at residue 431 early within Domain IV, as a result of programmed translational frameshifting (Fig. 1B) (12, 13). Domains IV and V are present in τ but absent in γ and provide for the connection between DnaB and the α subunit of Pol III, respectively. Residues 430-498 within Domain IV are responsible for binding DnaB (11), while Domain V and specifically C-terminal residues, 611 to at least 636, interact with α (14-16). Structured globular Domains I-III within the core of the CLC are connected to Domains IV/V through an unstructured long linker, giving flexibility and mobility for τ to interact with other proteins and respond to dynamic events occurring within the replisome. The CLC can contain two to three τ subunits (along with $\delta\delta'\psi\chi$) (15, 16). Therefore, the leading and lagging strand Pol III's can be linked through two τ subunits within the same CLC (17), and DnaB can be linked to the leading strand Pol III through one of those τ subunits (5). A third τ subunit can be utilized to recruit a third Pol III core in waiting for loading onto the next RNA primer for further Okazaki fragment synthesis *in vitro* (11), although genetic and cellular evidence favors a native $\tau_2\gamma_1$ -CLC *in vivo* (18-21).

The τ -mediated interaction between DnaB and Pol III enables the rate of coupled DNA unwinding and synthesis to approach ~1000 nt/s (5). In the absence of this coupling interaction, a molecular switch in the conformation of DnaB causes the translocation/unwinding rate to be reduced to ~35 nt/s (22). Uncoupling between the DnaB and Pol III can result in continued unwinding by the helicase but at a reduced rate of synthesis, leading to the accumulation of intervening ssDNA gaps (23). Blocks to replication may

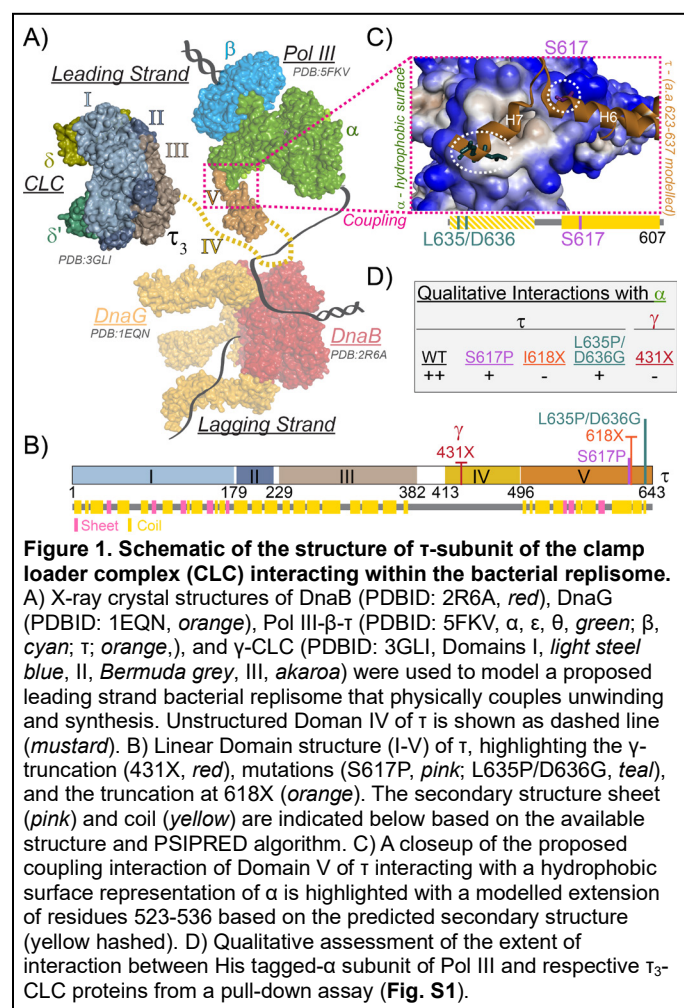


Figure 1. Schematic of the structure of τ -subunit of the clamp loader complex (CLC) interacting within the bacterial replisome.
 A) X-ray crystal structures of DnaB (PDBID: 2R6A, red), DnaG (PDBID: 1EQN, orange), Pol III- β - τ (PDBID: 5FKV, α , ϵ , θ , β , cyan; τ , orange), and γ -CLC (PDBID: 3GLI, Domains I, light steel blue, II, Bermuda grey, III, akaroa) were used to model a proposed leading strand bacterial replisome that physically couples unwinding and synthesis. Unstructured Domain IV of τ is shown as dashed line (mustard). B) Linear Domain structure (I-V) of τ , highlighting the γ -truncation (431X, red), mutations (S617P, pink; L635P/D636G, teal), and the truncation at 618X (orange). The secondary structure sheet (pink) and coil (yellow) are indicated below based on the available structure and PSIPRED algorithm. C) A closeup of the proposed coupling interaction of Domain V of τ interacting with a hydrophobic surface representation of α is highlighted with a modelled extension of residues 523-536 based on the predicted secondary structure (yellow hashed). D) Qualitative assessment of the extent of interaction between His tagged- α subunit of Pol III and respective τ_3 -CLC proteins from a pull-down assay (Fig. S1).

be caused by DNA damage, interfering transcription machinery, or tension in the supercoiled template (24, 25). Specifically, blocks to leading strand synthesis may result in decoupling with DnaB as unwinding/translocation continues on the lagging strand. Should replisome decoupling occur, an excess of ssDNA can be filamented by RecA triggering an SOS response that induces the expression of error prone DNA polymerases and other DNA repair enzymes attempting to mitigate this stress (23, 26).

For DNA replication to occur with high fidelity and efficiency, it is imperative that the synthesis of nascent strands occur immediately after DNA unwinding, thus reducing accumulation of labile ssDNA that could cause significant genomic instability. To further understand the genomic and cellular importance of this replisome coupling phenomenon, *dnaX* mutations corresponding to specific amino acid changes in the C-terminal helix-turn-helix motif of τ and predicted to weaken the induced interaction with the α -subunit of Pol III (15) were created (Figs. 1B-C & S1). *dnaX:mut* strains showed significant increases in cellular stress that included extreme cellular elongation, reduced growth rates, compromised fitness, increased SOS, and increased mutagenesis. In particular, *dnaX:L635P/D636G* displayed more deleterious effects overall than *dnaX:S617P*. Although all τ_3 -CLC mutants stimulated DnaB unwinding in isolation, and τ_3 -CLC(S617P) and τ_3 -CLC(L635P/D636G) performed leading strand synthesis at rates similar (or even greater) to WT, their ability to dilate DnaB to traverse over duplex DNA was impaired. This regulation switch of τ_3 -CLC in coordinating both Pol III recruitment and regulating DnaB unwinding plays an important role in maintaining efficient replisomal coupling of DNA unwinding and synthesis. Altogether, at least the C-terminal 26 residues of τ coordinate unwinding and synthesis within the replisome to maintain genomic stability in the bacterial cell.

Results

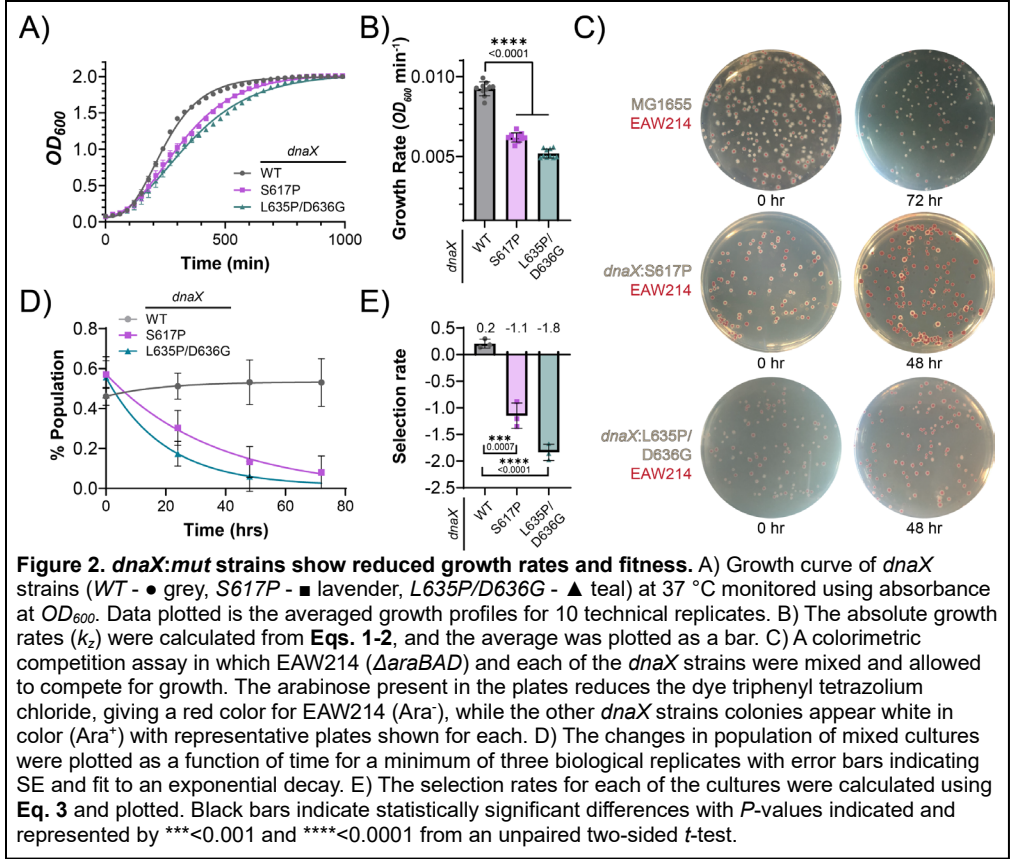
dnaX mutations limit growth, fitness, and viability

Previous work mapping the τ - α interaction concluded that upon binding, contacts occur through a structured helix (H6) which may induce previously unstructured residues 624-635 to adopt an additional downstream α -helix (H7), creating a helix-turn-helix motif (Fig. 1C) (15). They further concluded that these last 18 residues of τ (a.a. 626-643) are utilized for the interaction with α , in which the last 11 (a.a. 626-636) are required, and the last 7 (a.a. 630-636) are influential. Within that stretch of amino acids, they also identified several suppressor mutations to the growth inhibition found by overexpressing Domains IV-V that allowed binding to α with modest changes to binding free energy ($\Delta\Delta G$), including S617P (4.1 kcal/mol) and L635P or D636G (1.7 or 1.9 kcal/mol each). Before creating CRISPR/Cas9 edits in the *dnaX* gene to test replisome coupling, we made and tested full-length mutants of τ : S617P, L635P/D636G, and truncated τ , I618X, for qualitative binding interactions with the α -subunit of Pol III using nickel pull-down assays. The intensity of the protein bands coeluting were quantified to obtain fractional saturation values as a ratio of τ (or γ) to α bands (Fig. 1D & S1). WT τ showed the highest fractional saturation value indicating the strongest interaction with α , while L635P/D636G and S617P had reduced fractional saturation values, exhibiting weaker interactions with α . The control C-terminal truncation, I618X, deleting the last 25 amino acids, showed negligible binding with α , similar to γ , consistent with previous more quantitative analyses (15).

These same τ protein mutations were genetically edited in *dnaX* using CRISPR/Cas9 in the parental strain, MG1655. To increase the efficiency of recombination of a synthetic oligonucleotide containing the desired mutation and a novel restriction site for screening, the λ -red genes were exogenously induced. An outright deletion of the C-terminal residues of τ (*dnaX:I618X*) seemed likely to fail based on this previous evidence for its importance (15) and was evidenced by our several unsuccessful attempts to isolate this strain. However, several successfully edited mutated colonies were produced for (*dnaX:S617P* and *dnaX:L635P/D636G*) as screened by colony PCR and restriction digest (Fig. S2). These *dnaX:mut* strains were cured of pRedCas9 by growth at 42 °C to target the temperature sensitive origin, p15A to isolate the new strains. The strains were confirmed by whole genome sequencing to contain only the desired mutations and not any other obvious suppressors (Table S4).

Mass doubling times for all *dnaX:mut* strains were monitored at OD_{600} in 96 well plates using a plate reader at 37 °C. The growth rates can be suboptimal using this method which restricts aeration, but the assay is internally controlled and can be conveniently monitored and compared. The absolute growth rate (k_z) for the parental MG1655 stain is $9.2 \pm 0.4 \times 10^{-3} \text{ min}^{-1}$ and is consistent with previous studies using other instruments and strains (27). However, the rates for both *dnaX:S617P* ($6.2 \pm 0.3 \times 10^{-3} \text{ min}^{-1}$) and *dnaX:L635P/D636G* ($5.2 \pm 0.3 \times 10^{-3} \text{ min}^{-1}$) are significantly reduced (Fig. 2A-B).

As the *dnaX:mut*s had slower overall growth rates, we hypothesized that their relative fitness compared to the parental strain would also be reduced. To compare the fitness rates between two strains, a colorimetric growth competition assay was performed. A parental strain with a deletion of the arabinose isomerase promoter (EAW214: MG1655:ΔaraBAD) turns red from the inability to utilize the reducing sugar, arabinose, which converts triphenyltetrazolium chloride (TTC) to red formazan on the agar plates (27, 28). On the same plates, *dnaX:mut*s (*ara*⁺) degrade arabinose, leaving TTC oxidized (colorless) and produce typical white colonies (Fig. 2C). As an initial control, EAW214 (*ara*⁻) and MG1655 (*ara*⁺) strains were cocultured and plated on successive days and show consistently equal populations over 48-72 hours, while both *dnaX:mut* strains declined in population relative to EAW214 (Fig. 2D). In fact, to maintain an equal population of colonies on day 0, a 4:1 mixture ratio of *dnaX:L635P/D636G* to EAW214 was required for the initial coculture. The selection rates for each of the strains were quantified where *dnaX:S617P* and *dnaX:L635P/D636G* had negative selection rates of -1.1 ± 0.1 and -1.8 ± 0.1 , respectively, indicating severely reduced fitness compared to parental strains (Fig. 2E).



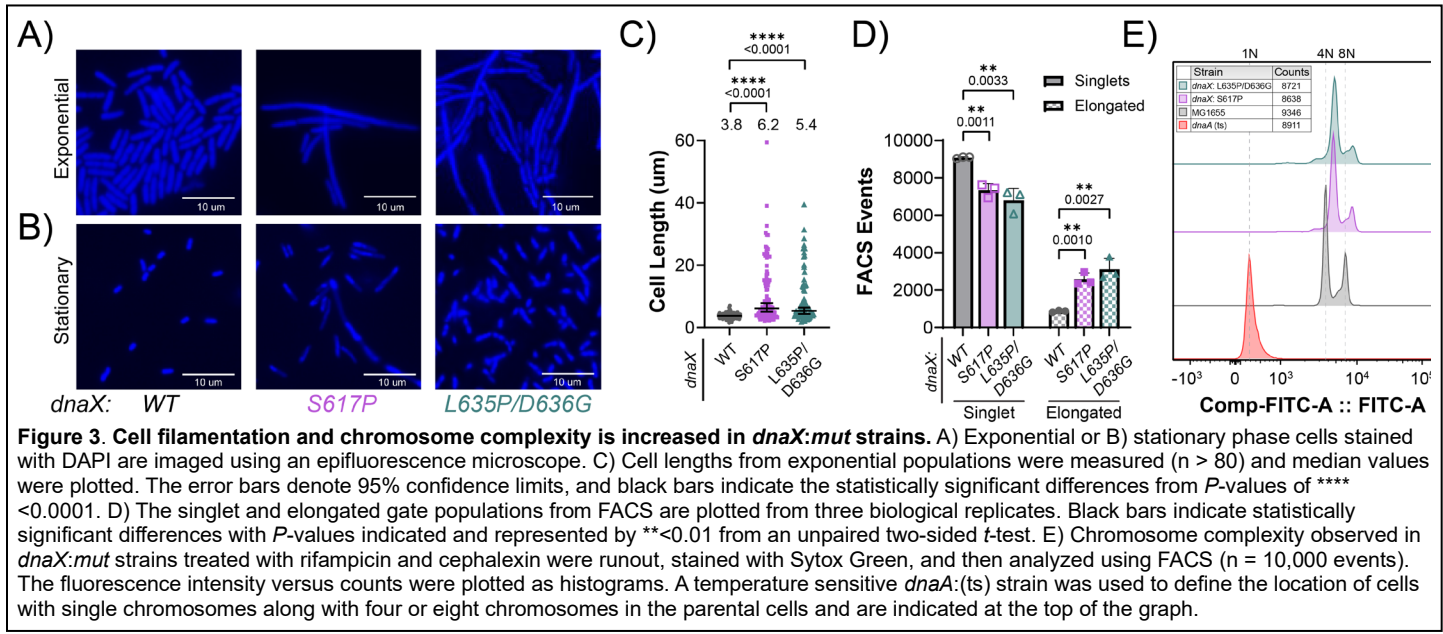
and plated on successive days and show consistently equal populations over 48-72 hours, while both *dnaX:mut* strains declined in population relative to EAW214 (Fig. 2D). In fact, to maintain an equal population of colonies on day 0, a 4:1 mixture ratio of *dnaX:L635P/D636G* to EAW214 was required for the initial coculture. The selection rates for each of the strains were quantified where *dnaX:S617P* and *dnaX:L635P/D636G* had negative selection rates of -1.1 ± 0.1 and -1.8 ± 0.1 , respectively, indicating severely reduced fitness compared to parental strains (Fig. 2E).

dnaX:mut show signs of cellular and genomic stress

As a phenotypic consequence, cellular or genomic stress can be reflected as changes in cell size or lengths. To confirm and quantify whether *dnaX:mut* cells have altered cellular morphologies, exponential and stationary phases were stained with DAPI and imaged. In exponential growing cells, both mutants, *dnaX:S617P* and *dnaX:L635P/D636G*, showed significantly elongated cells with median cell sizes of 6.2 and 5.4 μ m respectively compared to the parental strain with a median cell size of 3.8 μ m (Fig. 3A & C). Interestingly, there were several cells with vastly elongated lengths of greater than 30 μ m in each of the *dnaX:mut* strains. In stationary phase cells, the median cell length for the parental strain reduced to 1.8 μ m, while the median cell lengths of *dnaX:S617P* and *dnaX:L635P/D636G* in stationary phase were only reduced to 4.7 and 3.0 μ m respectively and were significantly longer than the parental strain (Fig. 3B & S3). To more globally assess cellular filamentation, we utilized FACS to quantify the subpopulations of singlets or elongated cells out of 10,000 events (Fig. 3D). Interestingly, both *dnaX:mut*s show significant increases in the proportion of elongated cells, 26.0 % for *dnaX:S617P* and 31.4% for *dnaX:L635P/D636G* compared to the parental strain of 8.8%, similar to the microscopy results.

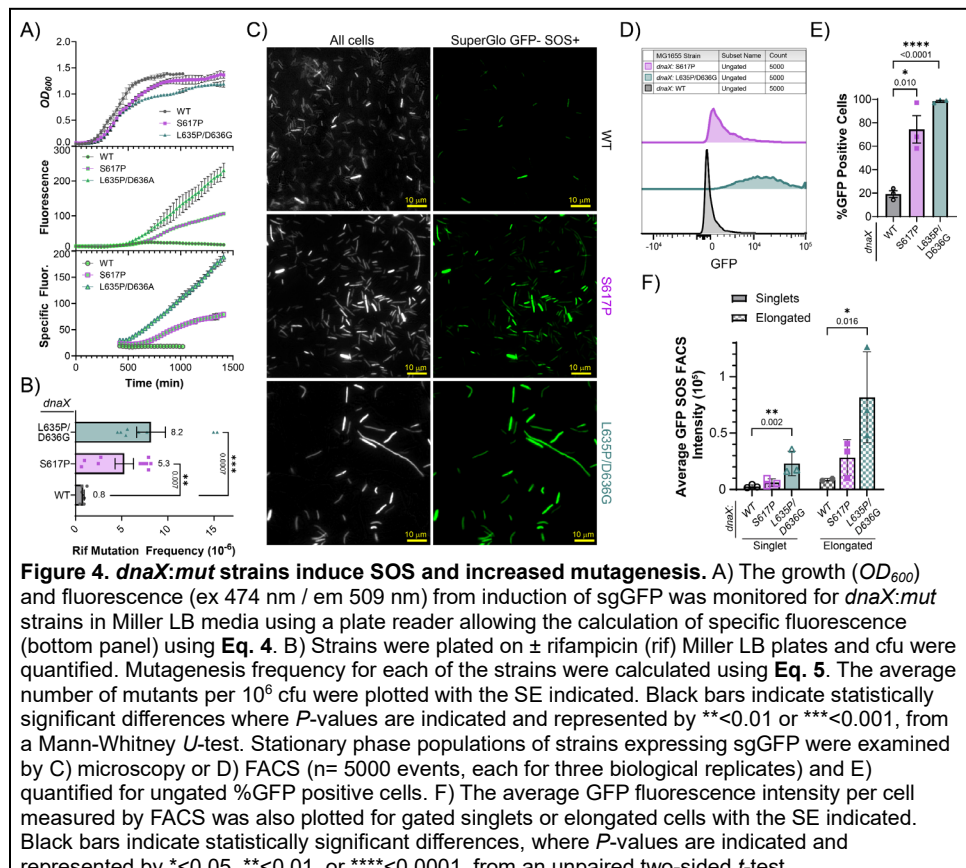
Cell filamentation observed in *dnaX:mut* strains may indicate inefficient replisome activity or genomic stress and result in a delay in fission. Generally, synchronized bidirectional replication in *E. coli* will result in 2^n number (n being any integer value) of chromosomes in exponentially growing cells (29). Treatment with rifampicin and cephalexin inhibits initiation of replication and cell division, respectively. A growth runout for 4 hours gives cells sufficient time to complete of ongoing rounds of replication before analysis of chromosome content by FACS (Fig. 3E & S4) (30). In the MG1655 strain, 2 major peaks are observed, correlating to 4 and 8

number of chromosomes; however, *dnaX:mut* strains contain a minor peak less than 4 chromosomes, indicating a delay in synthesis; a major peak greater than 4 chromosomes, indicating asynchronous replication initiation; and a minor broader peak corresponding to 8+ chromosomes, indicating overreplication or severe chromosomal excess or entanglement. Therefore, both *dnaX:S617P* and *dnaX:L635P/D636G* induce significant challenges for efficient and synchronous DNA replication that result in grossly abnormal chromosomal content.



Induction of SOS causes increased mutagenesis in *dnaX:mut* strains

Disruption in replisome coupling can lead to a large accumulation of ssDNA that triggers an induction of the SOS response to promote cellular survival (25). This SOS response results in the expression of a set of genes that work to delay cell division to repair any DNA damage (31). To determine whether the *dnaX:mut* strains induce SOS created from uncoordinated helicase unwinding and polymerase synthesis even in the absence of DNA damaging agents, they were transformed with a vector expressing SuperGlo GFP (sgGFP) under control of the *recN* promoter to monitor SOS induction (32). Strains were grown in the absence (Fig. 4A) or presence (Fig. S5) of a low dose of mitomycin C (MMC), and the specific fluorescence was calculated [30]. Specific fluorescence is used to account for the increase in cell density due to growth over time. The *dnaX:mut* strains exhibited dramatic increases in SOS induction in both



the absence and presence of MMC compared to the parental strain. *dnaX:L635P/D636G* showed the highest specific fluorescence over time in both nontreated and MMC treated conditions, but *dnaX:S617P* also showed a substantial increase in GFP signal associated with SOS in both scenarios. *dnaX:WT* as expected had minimal specific fluorescence over time in nontreated conditions and increased slightly over time under the low dose MMC treatment.

As SOS induction also facilitates an increase in mutagenicity by increased expression of error prone DNA polymerases, we wanted to examine the mutational frequencies of these *dnaX:mut* strains after exposure to rifampicin. Mutations arising in the *rpoB* gene, encoding for the β subunit of RNA polymerase, confers resistance to rifampicin (33). By quantifying the frequency of rifampicin mutagenesis, the mutagenicity of strains during heightened SOS can be determined (34). The parental strain had an average of 0.8 ± 0.1 mutation events per 10^6 number of cells (Fig. 4B), consistent with previous results (27). However, both mutant strains, *dnaX:S617P* and *dnaX:L635P/D636G*, showed significantly higher mutation rates than the parental strain with 8.2 ± 1.6 and 5.3 ± 1.0 mutation events per 10^6 cells, respectively.

To better visualize the abundance of SOS in untreated exponential cell populations, we examined sgGFP expression by microscopy and FACS. Both *dnaX:S617P* and *dnaX:L635P/D636G* showed significant GFP expression in most all cells, independent of an obvious subpopulation that were filamented (Fig. 4C). FACS was used to quantify GFP expression in cells and showed that both *dnaX:S617P* ($74 \pm 12\%$) and *dnaX:L635P/D636G* ($98 \pm 1\%$) had a significantly higher number of cells that were GFP positive compared to *dnaX:WT* ($19 \pm 3\%$) (Fig. 4D-E). Interestingly, not only were the fraction of GFP positive cells increased in both the singlets and elongated cells, but the average absolute fluorescence intensities were also increased in those subpopulations, indicating a massive increase in SOS induction (Fig. 4F & S6).

Increased ssDNA gaps are present in *dnaX:mut* strains

As the SOS response is a consequence of accumulation of significant ssDNA gaps coated by RecA, a Pol I dUTP Gap filling (PLUG) assay was utilized to visualize the ssDNA gaps *in situ* (23, 35). Fixed and permeabilized cells were treated with Klenow fragment (Polymerase I – 5' - 3' exonuclease deficient variant) and nucleotides that included BrdU that allowed gap filling extension to occur. Afterwards, filled gaps were marked by immunofluorescent probing of BrdU incorporation. For qualitative measurements, cells were visualized by fluorescent microscopy and both *dnaX:mut* strains appeared to show a greater number of BrdU foci, representing ssDNA gaps, when compared to *dnaX:WT* (Fig. 5A). To more thoroughly quantify BrdU labeling, the cells were analyzed by flow cytometry. Altogether, the ungated cell populations of *dnaX:S617P* and *dnaX:L635P/D636G*, had 30.7 and 42.3% of the cells labeled for BrdU, respectively, compared to only 15.6% of the WT population (Fig. 5D). Because both *dnaX:S617P* and *dnaX:L635P/D636G* showed increased

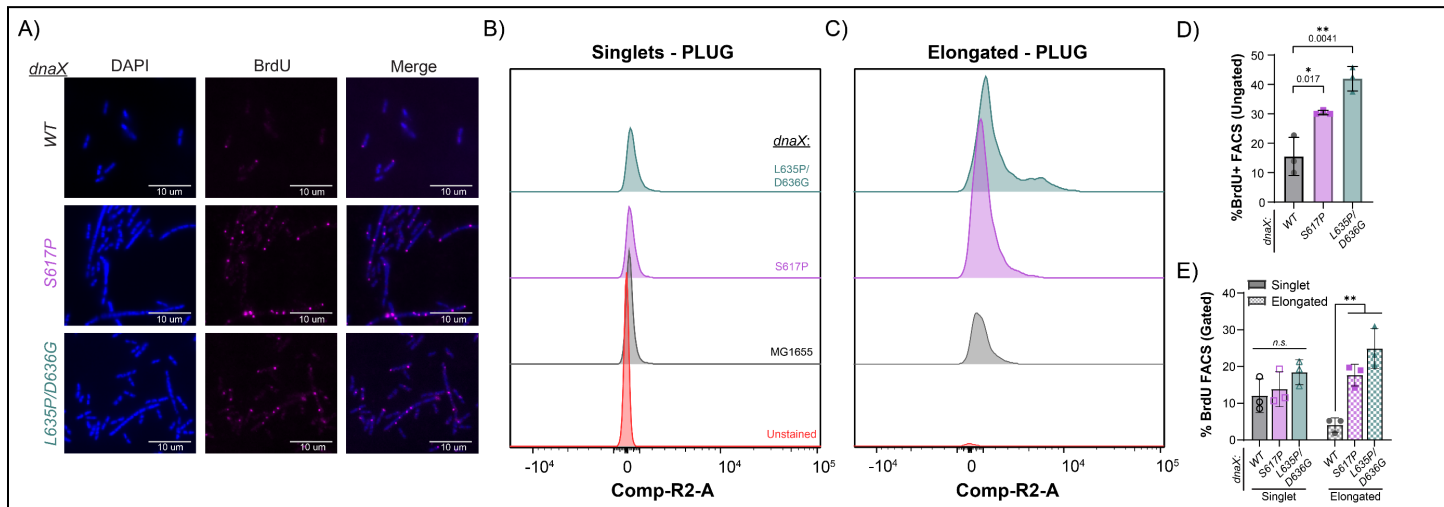


Figure 5. Increased ssDNA gaps are present in elongated *dnaX:mut* cells. A) Exponential phase cells were treated with Klenow polymerase and BrdU *in situ*, probed for BrdU in a PLUG assay, and imaged using immunofluorescence microscopy. Blue – DAPI panel represents DNA staining and Pink – BrdU represents ssDNA gaps. The fluorescence intensity of the cells for BrdU positive were also quantified using FACS ($n = 10\,000$ events, each for three biological replicates) and the histograms for gated cells are shown B) for singlets C) elongated cells. Quantification of the %BrdU positive PLUG cells for the D) ungated population or E) comparing singlets and elongated cells are plotted with the SE indicated. Black bars indicate statistically significant differences, where P -values are indicated and represented by $* < 0.05$ or $** < 0.01$ from an unpaired two-sided t -test.

cell filamentation (Fig. 3A-D), BrdU positive cells were gated and categorized into two populations: singlets and elongated (Figs. 5B-E & S7). Of these singlet events, 12.0% of *dnaX:WT* cells were positive for BrdU, and both *dnaX:S617P* and *dnaX:L635P/D636G* had slightly increased BrdU positive percentages for singlet cells of 13.8% and 18.4% respectively (Fig. 5E). Interestingly, *dnaX:S617P* and *dnaX:L635P/D636G* had significantly greater percentages of BrdU positive elongated cells (17.6 and 24.9% of the total cell population) compared to 4.1% for the WT cells (Fig. 5E). In fact, 67.9 and 79.1% of elongated *dnaX:S617P* and *dnaX:L635P/D636G* cells, respectively, were BrdU positive.

dnaX:mut strains have significantly more cell death

To investigate whether significant cell death in the *dnaX:mut* strains, likely from overwhelming single-strand DNA gaps and SOS, is contributing to measured slower growth rates, flow cytometry and microscopy were utilized to quantify populations of live and dead cells stained with SYTO9 and propidium iodide (PI) in late exponential stage (Fig. 6A). The percentage of dead cells measured by flow cytometry in S617P (10.4%) or *dnaX:L635P/D636G* (13.4 %) were significantly higher than WT (2.3%) (Fig. 6B & S8). Interestingly, both *dnaX:S617P* and *dnaX:L635P/D636G* exhibited a significant proportion of elongated cells that were PI positive (Fig. S8), which were also evident in the microscopy images (Fig. 6A). The more intense red color observed in the elongated cells is reflected in the flow cytometry data, where 38.7% and 51.0% of cells gated outside of the singlet population in *dnaX:S617P* or *L635P/D636G* were not viable (Fig. 6C).

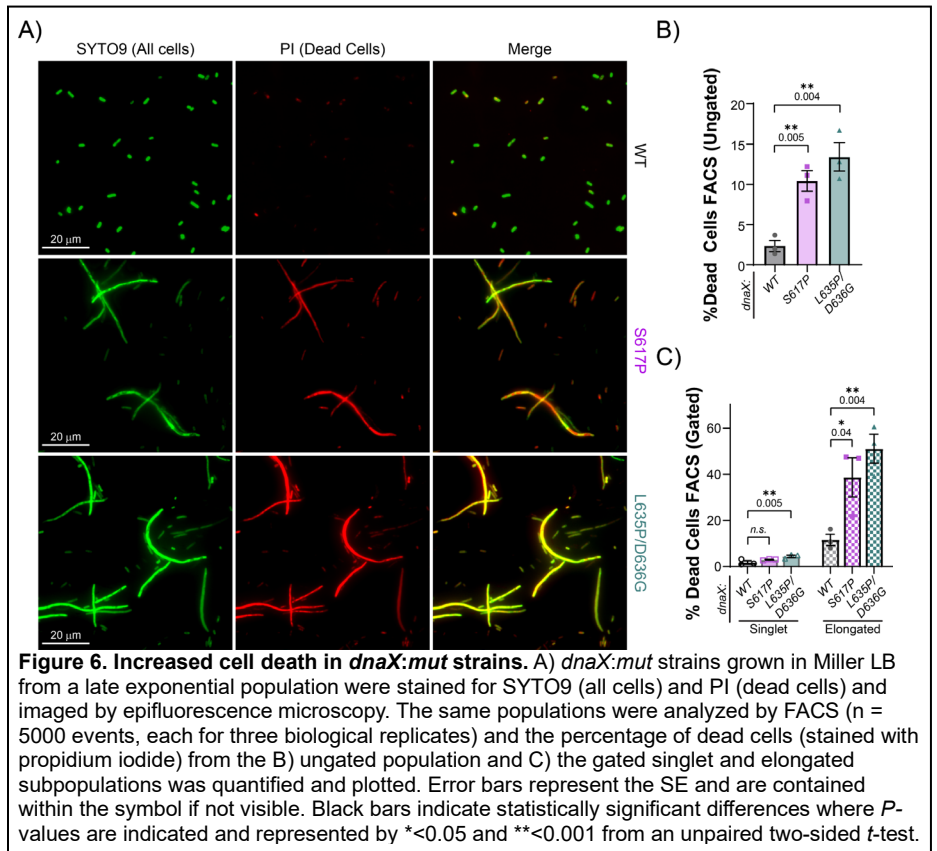


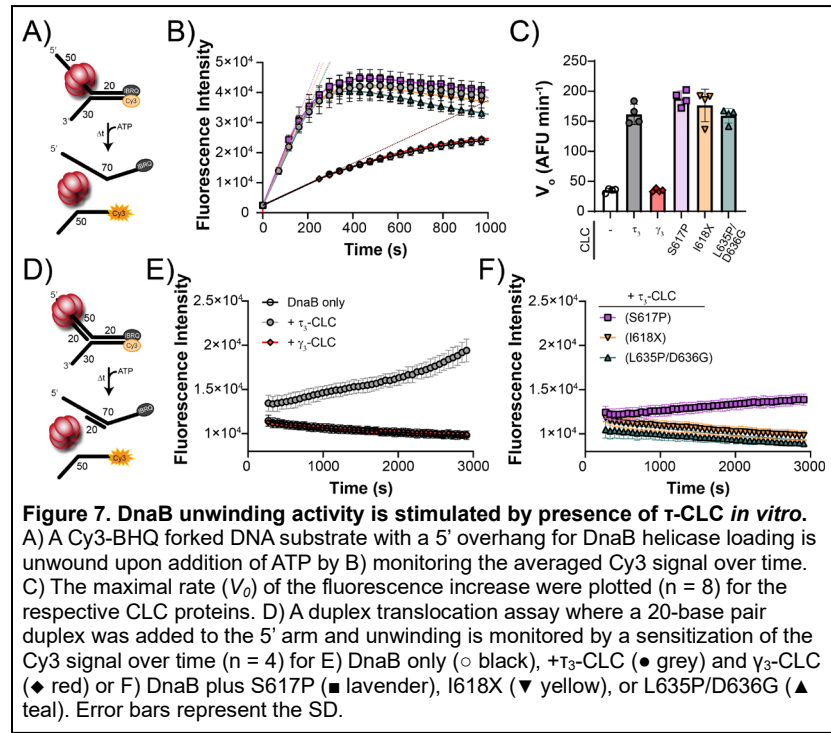
Figure 6. Increased cell death in *dnaX:mut* strains. A) *dnaX:mut* strains grown in Miller LB from a late exponential population were stained for SYTO9 (all cells) and PI (dead cells) and imaged by epifluorescence microscopy. The same populations were analyzed by FACS ($n = 5000$ events, each for three biological replicates) and the percentage of dead cells (stained with propidium iodide) from the B) ungated population and C) the gated singlet and elongated subpopulations was quantified and plotted. Error bars represent the SE and are contained within the symbol if not visible. Black bars indicate statistically significant differences where P -values are indicated and represented by * <0.05 and ** <0.001 from an unpaired two-sided t -test.

CLC stimulates DnaB unwinding in vitro

Examining the impact of perturbed τ - α interactions *in vivo* gave a more global representation of the negative effect that disrupting coupling had on gross genomic stability. However, to obtain a mechanistic explanation for the importance of τ - α interactions, purified τ_3 -CLC mutants were used in *in vitro* assays. In addition to S617P and L635P/D636G, a truncated τ_3 (I618X)-CLC was purified as a control that deletes the last 25 amino acids of the C-terminus that primarily interacts with α subunit (Fig. S9A).

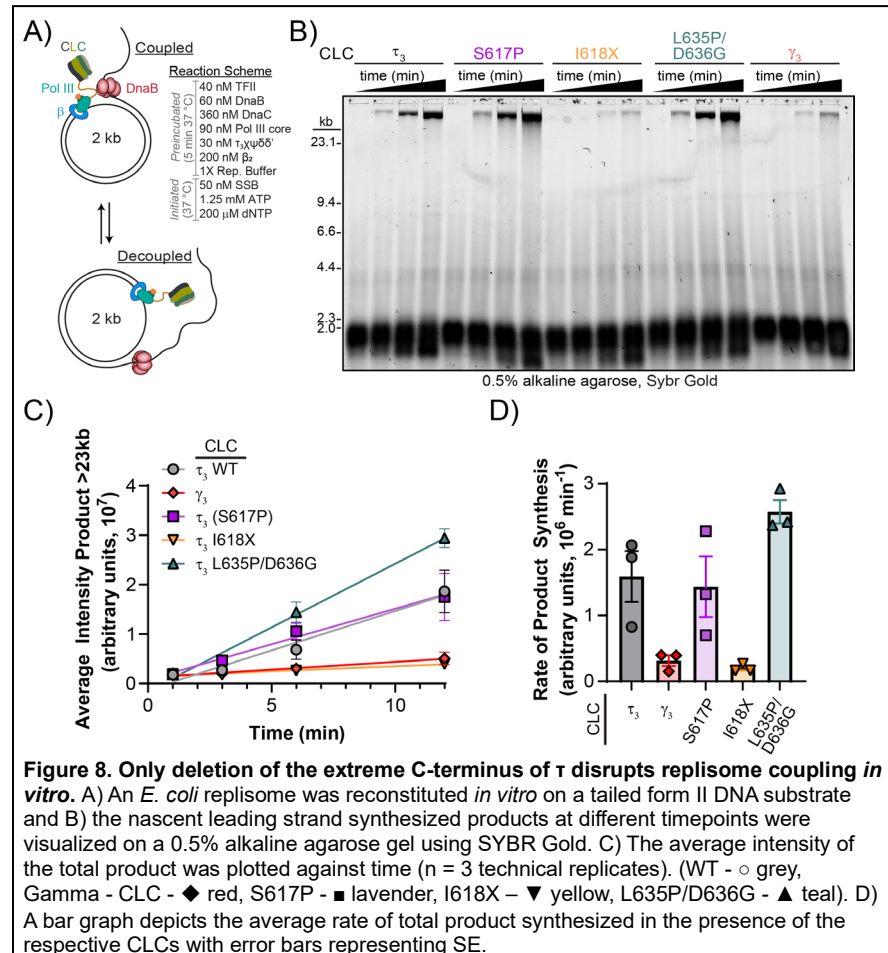
The sequence shared by both τ and γ proteins enables any of the associated CLCs to load the β clamp on DNA in an ATP-dependent manner (36, 37). Therefore, to verify that the activity of the purified mutated CLC proteins are not affected, a NADH-coupled ATPase clamp-loading assay was performed. As expected, all mutant CLC proteins including γ_3 -CLC showed similar ATPase activity, verifying that the CLC proteins were active (Fig. S9B). τ -DnaB interactions are also necessary to maintain a stable but dynamic replisome necessary for efficient fork progression connected through Domain IV, which is absent in γ_3 -CLC but present in all other τ_3 -CLC mutants (Fig. 1) (5, 11). A fluorescent DNA unwinding assay using a quenched forked substrate in the presence of DnaB helicase and the mutant CLC proteins was performed to analyze any stimulation of unwinding activity upon interaction with τ_3 -CLC (Fig. 7A). Both DnaB on its own or in the presence of γ_3 -CLC, had low unwinding rates; however, inclusion of other mutant τ_3 -CLC proteins all stimulated DnaB unwinding similar to that for WT τ_3 -CLC (Fig. 7B-C).

Like the duplex unwinding assay, the same BHQ-Cy3 forked substrate was utilized with the addition of a short 20 mer strand that anneals to the 5' arm to test the duplex translocation ability of DnaB prior to unwinding (Fig. 7D). DnaB on its own is unable to effectively translocate over this duplex region and unwind the fork; however, the addition of τ_3 -CLC helps to dynamically alter the DnaB hexamer conformation towards a dilated state, allowing duplex translocation followed by effective fork unwinding (Fig. 7E). Domains IV and V of τ_3 -CLC are also important for inducing a dilated state in DnaB as γ_3 -CLC is unable to facilitate duplex translocation. Like γ_3 -CLC, τ_3 (I618X)-CLC and τ_3 (L635P/D636G)-CLC are unable to induce dilation of DnaB for duplex translocation. However, τ_3 (S617P)-CLC does allow for about one-third of the rate of DnaB dilation/translocation compared to WT (Fig. 7F). Therefore, structural features within Domain V of τ propagate through to Domain IV to impact the DnaB hexamer conformation for effective duplex translocation, and these τ mutants have a reduced ability to alter the DnaB conformation.



Leading strand synthesis decouples when τ – Pol α interactions are fully disrupted

To directly test whether disruption in replisome coupling results from mutations of the τ - α interface, mutant τ_3 -CLC proteins were utilized in a reconstituted *in vitro* leading strand replisome assay (Fig. 8A). Previously it was shown that the τ -mediated physical interaction between helicase and polymerase is required for the high rate of replication fork progression (5). The tailed form II rolling circle substrate (TFII) is a nicked circular DNA template with a 5' overhang that mimics an open replication fork, making it an ideal substrate to study DNA replication *in vitro* (38). Utilization of γ_3 -CLC or τ_3 (I618X)-CLC complexes in this rolling circle assay resulted in a significant reduction in overall leading strand product compared to a WT τ_3 -CLC complex (Fig. 8B-C). Interestingly, both τ_3 (S617P)-CLC and τ_3 (L635P/D636G)-CLC showed similar (if not slightly elevated) leading strand products compared to WT. It appears that only



complete disruption of the τ - α interface through deletion of the last 25 amino acids (i.e. I618X) fully inhibits the leading strand replisome, while moderate perturbation at the interface (S617P or L635P/D636G) are not sufficient to disrupt coupling in this ideal *in vitro* system where DnaB dilation is generally unnecessary.

Discussion

The model of a stable replisome and uninterrupted DNA replication process from origin to terminus has been recently challenged by the discoveries of more dynamic replisome components (10, 39). Even so, the DnaB helicase has the longest dwell time bound to DNA in comparison to the other replisome proteins and is believed to act as the stable platform upon which the rest of the components reassemble (6). The Pol III* subassembly ($\alpha\epsilon\theta\tau_3\delta\delta'$, without the β -clamp) is frequently exchanged with Pol III* in solution, and for this exchange to occur, at least one τ -subunit should be present in the CLC (6, 7, 40). Furthermore, the rate of DNA synthesis is kinetically discontinuous with frequent pausing, during which DNA unwinding slows down to allow recoupling with the polymerase (9). Therefore, by altering the speed of helicase unwinding, kinetic coupling can be maintained through physical coupling with the polymerase to limit the production of ssDNA gaps (9, 27). With Pol III* being constantly exchanged in a concentration dependent manner, it is important to maintain and regulate a physical link to the more stable helicase hub through τ to couple unwinding with synthesis.

Previous studies have shown that the C-terminus of τ consists of a structured region within Domain V (residues 507 – 617, H6 in **Fig. 1C**), but is unstructured beyond S617 unless it is bound to α (modeled H7 in **Fig. 1C**) (15, 16). S617P is located near the end of the first α -helix (H6) that interacts directly with the α -subunit of Pol III, and substitution of Ser to Pro, would likely disrupt the entire H6 and/or destabilize binding of the downstream induced β -turn-H7 reducing affinity with α . The induced H7 α -helix spans from N622 to D636 and is modeled to interact within a hydrophobic patch on α (15). In addition to S617P, we chose to either terminate τ at I618X or combine mutations (L635P and D636G) in the induced H7 to better understand how interactions between α and τ through H6 and H7 couple and regulate DNA synthesis and unwinding to prevent genomic instability during replication.

The parental strain MG1655 was genetically engineered to introduce targeted mutations in the *dnaX* gene corresponding to S617P and L635P/D636G mutations in the τ protein, to perturb (but not eliminate) Pol III α - τ interactions occurring at the C-terminus of τ . Although we made several attempts to edit *dnaX*:I618X, we could never recover any successful clones, highlighting the importance of the downstream H6 and H7 interactions with α required for survival. Previously, deletion of the last 7 (Δ 636-643) or 11 (Δ 632-643) residues moderately or severely inhibited the interaction with α , even though these residues are past H6 (15). The two successfully edited *dnaX*:*mut* strains both showed reduced growth rates, fitness, and survival rates in addition to increased levels of SOS and mutagenesis. Reduced growth rates and fitness in both mutant strains indicate that by altering the α - τ interaction, there are adverse impacts on the continuity of DNA replication, cell segregation, and strain survival.

dnaX:*mut* strains displayed altered cell morphologies and increased odd numbers of chromosomes corresponding to asynchronous replication. Elongated cellular filamentation is a phenotypic indication of cellular stress (41), and asynchronous replication can generate complex genomic intermediates and stretches of unreplicated DNA. In defense, the SOS response will be upregulated to inhibit cell division by expression of *sulA* to allow for the resolution of any unreplicated DNA through increased expression of DNA repair genes, including the translesion polymerase, Pol V (42, 43). It was evident that these *dnaX*:*mut* strains had higher levels of ssDNA gaps as detected by PLUG, confirming that targeted decoupling leads to abundant ssDNA gaps. Those ssDNA gaps activated the SOS response in an attempt at survival but also resulted in increased chromosomal complexities, indicative of severe genomic damage and explaining the severely elongated cellular phenotypes. Cellular elongation generally persisted into stationary phase in these strains, consistent with a slow replication/repair phenotype and also reflecting severe and adverse genomic complications. *dnaX*:*mut* strains also had reduced survival rates, with a larger proportion of non-viable cells in the elongated subpopulations. Therefore, this establishes a pattern whereby persistently disrupted replisomal coupling leads to accumulation of ssDNA gaps, resulting in SOS induction and cellular filamentation ultimately overwhelming the genomic repair process and ending in cell death.

We expected that by altering the τ - α interactions, replisome coupling between unwinding and synthesis will be primarily affected, resulting in these genomic and cellular markers of stress, but τ also interacts with DnaB (primarily through Domain IV). This τ -DnaB interaction can also affect the speed of helicase in controlling

replisome progression, where τ can bring about a conformational change in DnaB that allows it to unwind faster (5, 44). Interestingly, while WT and mutant τ_3 CLC proteins were all capable of stimulating DnaB unwinding to varying degrees, only WT CLC was able to effectively allow a conformational change in DnaB to dilate and translocate over dsDNA. This constricted-dilated DnaB regulation may be one of the most important factors for maintaining an effective and dynamic replisome (27).

Interestingly, τ_3 -CLC(L635P/D636G) was capable of both stimulating DnaB unwinding and synthesizing leading strand products at levels even in excess of WT but did not allow for effective DnaB dilation over duplex DNA. τ_3 -CLC(S617P) had a much-reduced ability to dilate DnaB, likely explaining why *dnaX:S617P* exhibited less extreme phenotypes *in vivo* compared with *dnaX:L635P/D636G*. *dnaX:L635P/D636G* exhibits the greatest frequency of dead cells, mutations, SOS induction, and single strand gaps, leading to the most significant cellular elongation and slower growth phenotypes. We suspect that the extreme C-terminus of τ not only acts as a primary interaction site with α but also as a regulation switch to help with Pol III* recycling, directly impacting DnaB unwinding regulation. In the absence of this regulation switch, Pol III* is not effectively recruited or evicted during rounds of lagging strand synthesis or leading strand blocks. For *dnaX:L635P/D636G*, this τ -CLC mutant stimulates the unwinding of DnaB but is unable to regulate the DnaB conformation to control the speed when Pol III* is needed or to overcome genomic obstacles *in vivo*, leading to increased ssDNA gaps and rampant cellular stress.

Replisome decoupling may occur because of several genomic challenges, disrupted replisome interactions, or the inability to induce conformational switching to control the kinetics as described previously (45). During decoupling, polymerase progression may be inhibited while releasing the helicase to continue unwinding, leaving regions of ssDNA exposed. Accumulation of excess ssDNA is a substrate for RecA binding and filamentation initiating the SOS response to induce gene expression of DNA repair genes that contribute to error prone DNA synthesis for survival (43, 46). τ acts as the lynchpin to physically connect the helicase and polymerase and is shown to play a multifaceted role in ensuring that coupling extends far beyond a mere physical connection but also impacting conformation. By regulating a transition between constricted and dilated states in DnaB, τ can control the unwinding speed to ensure the helicase and polymerase remain coupled despite constant polymerase recycling and differential enzymatic rates to maintain efficient replication and ensure genomic integrity.

Experimental Procedures

Cloning and Expression of τ -CLC Mutants

Mutations in the τ protein were introduced using primers containing the targeted mutation and novel restriction site (**Table S3**) in PCR reactions with pCOLADuet-1 containing the *dnaX* gene (47) as the template and Platinum SuperFi PCR Master Mix (ThermoFisher, Waltham, MA). Colonies were PCR screened and confirmed by restriction digested and whole plasmid sequencing (Plasmidsaurus, Eugene, OR). Confirmed mutant plasmids were transformed into Rosetta2 expression cell line and overexpression of $\tau_3\delta\delta'\psi\chi$ was induced with IPTG (1 mM). Purification of the CLC complexes were performed as previously described (47).

Bacterial CRISPR-Cas9 Genome Editing

The parental *E. coli* strain, MG1655, was used to create genetically edited CRISPR/Cas9 mutants of *dnaX* gene using a dual vector targeting system. Synthetic 40 base pair oligonucleotides with sequences homologous to *dnaX* targeting region acting as gRNA (**Table S3**) were ligated into the pCRISPR plasmid (Addgene: 42875) (48). First, pREDCas9 (Addgene: 71541) (49) was electroporated into MG1655 and plated on 100 μ g/mL spectinomycin (Gold Biotechnology Inc, St. Louis, MO) LB agar plates (10 g/L tryptone, 5 g/L yeast extract, 10 g/L NaCl, and 15 g/L agar) at 30 °C. Then both 100 ng of pCRISPR-g*dnaX* and 1 μ M of ssDNA oligonucleotides containing homologous region to *dnaX*, targeted single point mutations, and novel restriction sites for screening were simultaneously electroporated and plated on spectinomycin/kanamycin (50 μ g/mL) LB agar plates and incubated at 30 °C. Colony PCR followed by restriction digest was used to verify the presence of the novel restriction site (**Fig. S2**), ensuring successful genomic editing. These *dnaX:muts* were then allowed to grow at 42 °C in LB/Kan to cure the pREDCas9 plasmid from a temperature sensitive origin, p15A. The genomes of *dnaX:S617P* and *dnaX:L635P/L636G* were sequenced (Plasmidsaurus, Eugene,

OR) to further verify the single point mutations in the genome at the targeted site and eliminate the possibility of off-target mutations (**Table S4**). All further experiments were grown at 37 °C, unless specified otherwise.

τ – α pull down assay

Pull-down assays were performed by adding 50 μ L of nickel resin (HisPur™ Ni-NTA Resin, ThermoFisher) to a 1.5 mL Eppendorf tube and spun down at 800 xg for 2 min. The supernatant was removed, and the pellet was resuspended in 50 μ L of binding buffer [20 mM sodium phosphate, 0.125 M NaCl, 25 mM imidazole, 1 mM ATP, pH 7.4], spun down again, and the supernatant discarded. A 1:1 ratio of His-tagged Pol α to τ_3 -CLC are mixed with the resin and allowed to incubate at 4 °C for 30 min before spinning down and transferring the flow through (FT) solution to a new tube. The pellet was resuspended in 50 μ L of binding buffer, spun down, and transferred to a new tube as the first wash, taking care not to disturb the resin pellet. This wash step is repeated 12 more times (13 total) to ensure that all unbound protein is removed before resuspending the resin in 50 μ L of elution buffer [20 mM sodium phosphate, 0.125 M NaCl, 500 mM imidazole, pH 7.4], spinning down, and transferring the elution solution to a new tube. Finally, the FT, washes, and elution are electrophoresed on a 10% SDS Bis-Tris acrylamide gel, stained with Simplyblue Safestain (ThermoFisher, Waltham, MA), imaged on a Gel DocTM EZ system (Bio-Rad, Hercules, CA). The bands corresponding to τ and α were quantified separately using ImageQuant (v.10.2), and the fractional saturation was calculated by obtaining the band intensity ratio of τ (or γ) to α .

Growth Assay

Overnight cultures were diluted to reach an OD_{600} value ~ 0.01 and 200 μ l of diluted culture was aliquoted into white, clear bottomed 96 well plates and analyzed on a Tecan Spark microplate reader (Männedorf, Switzerland). The absorbance values were recorded at 30-minute intervals over 24 hours and the temperature was maintained at 37 °C with aeration at 240 rpm to control for regular growth profiles. Data was analyzed using GraphPad Prism (v10.2) and fit into a modified 4-parameter Gompertz growth model as follows:

$$w(t) = B + A^{-e^{\left(\frac{k_g \times 2.7182}{A} \times (T_{lag} - t) + 1\right)}} \quad (1)$$

where $w(t)$ is the density as function of time, B is the lower asymptote, A is the higher asymptote, T_{lag} is the lag time of the culture, t is time, and k_g is growth rate coefficient. The absolute growth rate (k_z) can be calculated using the following equation:

$$k_z = \frac{k_g \times 2.7182}{A} \quad (2).$$

The absolute growth rates were plotted and analyzed for any significant differences using unpaired two-tailed t-test with GraphPad Prism (v10.2).

Live/ Dead Analysis

To visualize and measure the viability of *dnaX:mut* strains, the LIVE/DEAD BacLight Bacterial Viability Kit L7012 (ThermoFisher, Waltham, MA) was used. Overnight grown cultures were diluted 100-fold in fresh Miller LB media and allowed to grow till OD_{600} reached late exponential phase (0.8~0.9). 25 mL of culture was centrifuged at 4000 x g for 20 minutes and the pellets were resuspended with 2 mL of 0.85% sterile NaCl solution. 1 mL of resuspended solution was added to 20 mL of 0.85% NaCl solution (70 % ethanol for dead cells as a control) and incubated at room temperature for 1 hour with mixing at 15-minute intervals. The samples were then centrifuged at 4000 x g for 20 minutes and resuspended in 20 mL of 0.85 % NaCl and centrifuge step was repeated. The pellets were resuspended in 10 mL of 0.85% NaCl, and 3 μ L of 1:1 mixture of SYTO9 (3.34 mM) and propidium iodide (PI) (20 mM) was added to 1 mL of resuspended bacterial suspension and incubated in the dark for 15 minutes.

For microscopy, 5 μ L of stained solution was added to the slide followed by 3 μ L of included mounting media, coverslip added, and sealed with clear nail polish. Microscopy images were visualized using Olympus Brightfield microscope IX-81 (Olympus Corp. Center Valley, PA) with a 60x objective lens upon oil immersion. Images were visualized with FITC filter for SYTO9 and TRITC filter for PI. The stained bacterial suspensions were used for analysis on the flow cytometer (Cytek Northern Lights flow cytometer, CA)

Competition assay

A derivative of MG1655, EAW214, containing an *araBAD* mutation within the promoter region was used as the control strain for this assay (gift from Mike Cox) (28). When plated on tetrazolium arabinose (TA) plates, the *ara*⁻ strains appear as red colonies as they cannot utilize arabinose as carbon source. TA plates contain 1 % arabinose (Oakwood products, Estill, SC) and 0.2 mg/mL triphenyl tetrazolium chloride (Sigma, St. Louis, MO). The *dnaX:WT* and EAW214 strains were mixed with equal numbers from an overnight culture. The *dnaX:S617P* and EAW214 strains were mixed in a 3:1 ratio, and *dnaX:L635P/D636G* and EAW214 were mixed in a 4:1 ratio, and diluted 10⁻⁶ in sterile water and plated on TA plates to ensure a 50:50 ratio of red:white colonies on Day 0. The mixed strains were diluted 100-fold in LB media and allowed to grow for 24 hours, diluted, and plated on TA plates. This procedure was repeated until there was a significant drop in one population of cells with respect to the competing population (27, 28). The selection rate of each of the strains were calculated using the following equation:

$$\text{selection rate} = r = \ln \frac{A_1}{A_0} - \ln \frac{B_1}{B_0} \quad (3)$$

where A_0 and B_0 are colony forming units (CFU) fractions of strains A and B at time 0 and A_1 and B_1 are CFU fractions of strains A and B after 24 hours. The selection rates were plotted and analyzed for significance using unpaired two-tailed t-test with GraphPad Prism (v10.2).

Microscopy

To examine exponential phase cells, overnight cultures were diluted 1000-fold and grown until OD_{600} reached ~0.4 before harvesting. Stationary phase cells were grown overnight. 1 mL of culture was pelleted, washed with PBS and resuspended in 70% ethanol. 2 μ L of the fixed cell samples followed by 3 μ L of staining and mounting solution containing DAPI (ThermoFisher, Waltham, MA), DABCO, glycerol and PBS were spotted onto microscope slides, covered with a coverslip, and sealed with clear nail polish. Microscopy images were visualized using an Olympus Brightfield Microscope IX-81 (Olympus Corp. Center Valley, PA), with a 60x objective lens upon oil immersion. Cell lengths were measured using cellSens software (Olympus, Center Valley, PA, USA). The cell lengths were plotted and analyzed for significance using a Mann-Whitney two-sided U-test with GraphPad Prism (v10.2).

Chromosome Content

Overnight grown cultures were diluted 1000-fold and allowed to reach an OD_{600} value of ~ 0.35 prior to treating with rifampicin (300 μ g/mL) and cephalexin (30 μ g/mL) and then allowed to grow out for 4 hours at 37 °C to complete chromosome synthesis (27). Cells were pelleted, washed in 1X TE buffer, and fixed in 70 % ethanol. Fixed cells were pelleted, washed, and resuspended in PBS containing 1.5 μ M of Sytox Green (Invitrogen, Carlsbad, CA) and allowed to stain for 30 minutes in the dark at room temperature. The stained samples were diluted with sheath fluid and analyzed by flow cytometry (BD FACSVerse flow cytometer, BD Biosciences, San Jose, CA). Unstained cell samples were used as a control to set the gating. Data was plotted using FloJo software (BD Biosciences). A temperature sensitive *dnaA(ts)* strain, CM742, carrying the *dna46* mutation was prepared as previously described (27).

SOS Induction

The plasmid, pEAW915, contains the SuperGlo GFP gene under the control of the *recN* promoter (gift from Mike Cox); a gene that is induced in the early phase of the SOS response (32). This reporter plasmid was transformed into *dnaX:mut* strains by electroporation. Overnight grown cultures were diluted 100-fold in LB media or LB media with 0.001 μ g/mL mitomycin C (ThermoFisher, Waltham, MA) and 200 μ L aliquots were added into white, clear bottomed 96-well plates. The cultures were incubated at 32 °C (to maintain normal growth profiles) and the absorbance (OD_{600}) and the fluorescence (ex 474 nm / em 509 nm) were read at 30-minute intervals over a course of 24 hours using Varioskan LUX microplate reader (ThermoFisher, Waltham, MA). For analysis, specific fluorescence was calculated using the following equation (32)

$$\text{Specific fluorescence} = \frac{\text{Fluorescence}}{\text{Absorbance (OD}_{600}\text{)}} \quad (4)$$

and the maximum fluorescence at equivalent times were analyzed for significant induction of SOS using a unpaired two-tailed t-test with GraphPad Prism (v10.2).

To analyze the cells using flow cytometry, 200 μL of overnight grown culture (stationary phase) was pelleted and washed thrice with 1x sterile PBS. The cells were resuspended in 1 mL of 1x PBS and analyzed using the flow cytometer (Cytek Northern Lights flow cytometer, CA). For microscopy, cells were prepared using the same procedure as for flow cytometry, with an additional step of fixing the cells with 4% paraformaldehyde in PBS and incubated at room temperature for 20 minutes. Followed by washing thrice with 1x PBS and resuspended in 500 μL of 1x PBS. 4 μL of the bacterial suspension was spotted on a slide and slides were prepared as mentioned previously. Slides containing SuperGloGFP transformed cells were visualized using an Olympus Brightfield Microscope IX-81 (Olympus Corp. Center Valley, PA), with a 60x objective lens upon oil immersion.

Rifampicin Mutagenesis Assay

Overnight grown cultures were diluted 1000-fold and allowed to grow for 24 hours before rediluting and growing for an additional 24 hours. 100 μL aliquots were plated on LB agar plates containing rifampicin (50 $\mu\text{g/mL}$) directly or serially diluted and plated on LB agar plates (50, 51). The rate of mutagenesis was calculated using the following equation:

$$\text{mutation frequency} = \frac{A}{B \times 10^6} \quad (5)$$

where A is the number of CFU on plates with rifampicin and B is the number of CFU on plates without rifampicin. The growth rates were plotted and analyzed for significance using unpaired two-tailed t-test with GraphPad Prism (v10.2).

Immunofluorescence assay

Overnight grown cultures were diluted 1000-fold and allowed to reach an OD_{600} value of ~ 0.5 , pelleted at 4000 $\times g$ for 15 minutes, the pellet was washed thrice with PBS, fixed with 1 mL of 4 % paraformaldehyde in PBS, and incubated at room temperature for 20 minutes. Following fixing, cells were pelleted, washed twice with PBS, and the cell pellets were resuspended in 70 % cold ethanol and stored at 4 $^{\circ}\text{C}$ until ready for immunolabeling. For the PLUG labeling assay, the cells stored in 70 % ethanol was pelleted, washed with PBS and resuspended in 100 μL of reaction buffer (5 U of Klenow fragment [NEB, Ipswich, MA], 1X NEBuffer 2, 10 μM each of dATP, dCTP, dGTP and 5-bromo-2'-deoxyuridine [BrdU, ThermoFisher, Waltham, MA]), and incubated at 37 $^{\circ}\text{C}$ for 30 minutes. The cell pellets were resuspended and washed twice in PBS, resuspended again in 100 μL of blocking solution of 4% BSA in 1X TBST [50 mM Tris and 150 mM NaCl, 0.1% Tween, pH 7.6], and incubated at 4 $^{\circ}\text{C}$ overnight on a rocker. The cells were pelleted and then resuspended in 100 μL of primary antibody solution with 1:100 mouse anti-BrdU (BD Biosciences, San Jose, CA) in 2% BSA in TBST and incubated at room temperature on a rocker for 1.5 hours. The cells were then pelleted and washed thrice with TBST and resuspended in 100 μL of secondary antibody solution with 1:500 goat anti-mouse IgG (H+L) AF647 (SouthernBiotech, Birmingham, AL) and incubated at room temperature on a rocker for 1.5 hours. The cells were pelleted, washed with TBST and resuspended in 1 mL of PBS.

To prepare the cells for microscopy imaging, 2 μL of the cells were spotted on clean microscope slides, and once dried, 2 μL of SlowFade DiamondAntifade Mountant with DAPI (ThermoFisher, Waltham, MA) was added, covered immediately with a coverslip, and sealed with clear nail polish. The slides were visualized using an Olympus Brightfield Microscope IX-81 (Olympus Corp. Center Valley, PA), with a 60x objective lens upon oil immersion. Both DAPI filters and Cy5 filters were used for visualization.

To analyze the fluorescence intensities, cells were diluted with sheath fluid and analyzed using flow cytometry (BD FACSVerse flow cytometer, BD Biosciences, San Jose, CA). Fixed cells that were unlabeled were used as a gating control to test for BrdU negative cells. Data was plotted using FloJo software (BD Biosciences).

Leading strand synthesis assay

In vitro leading strand DNA replication assays were performed with a reconstituted *E. coli* replisome (23) using the tailed-form II substrate for rolling circle amplification created from the vector pSCW01 as described (38). The fork oligonucleotide Cy5-DNA200 (IDT, Coralville, IA) (Table S3) was annealed to the gapped plasmid. DnaB and DnaC were purified as described (27, 52). *E. coli* SSB, β -clamp, and $\gamma_3\delta\delta'\psi\chi$ were generous gifts from Charles McHenry. Pol III core was purified as described (53).

For the replication assay, 40 nM DNA template was incubated with 30 nM $\tau_3\delta\delta'\psi\chi$, 90 nM Pol III core (α, ϵ , and θ), 60 nM DnaB (hexamer), 360 nM DnaC, and 200 nM β -clamp at 37 °C for 5 minutes in replication buffer (50 mM Tris-HCl pH 7.5, 10 mM MgCl₂, 10 mM (NH₄)₂SO₄, and 4 mM dithiothreitol [DTT]) and initiated with 1.25 mM ATP, 50 nM SSB, and 200 μ M dNTPs. The reactions were terminated with 1.5 μ L of 0.5 M EDTA and 3 μ L of DNA loading dye (6 mM EDTA, 300 mM NaOH, 0.25% [w/v] bromocresol green, 0.25% [w/v] xylene cyanol FF, 30% glycerol) after reaching their respective timepoints (38). Reactions were electrophoresed on 0.5% alkaline agarose gels in 1x alkaline agarose buffer at 15 V for ~15.5 hours. Gels were neutralized in 2x TAE for 2 hours on a rocker, stained with 1x SYBR Gold (Invitrogen) in 2x TAE for 2 hours, and imaged using GE Typhoon FLA 9000 (Cytiva, Marlborough, MA) for fluorescence. The bands in the gels were quantified using ImageQuant (v.10.2).

NADH-coupled ATPase assay

To verify the activity of mutant τ_3 -CLC proteins, a NADH-coupled ATPase assay was performed. The master mix was prepared with 1x reaction buffer (20 mM HEPES-KOH, 5 mM Mg(OAc)₂, 50 mM potassium glutamate, 5% glycerol, 0.2 mg/mL BSA, 4 mM DTT, pH 7.5), 2 mM ATP, 8 mM phosphoenol pyruvate, 480 nM NADH, 1 μ M ssDNA DNA165, and 3.6 μ L of pyruvate kinase/lactate dehydrogenase enzyme (Sigma, St. Louis, MO). The samples were aliquoted in to a 384-well black microplate (Corning) and initiated with 250 nM of β -clamp and 250 nM of the respective CLC protein. The fluorescence (ex 340 nm/ em 460 nm) was read at 30-second intervals over a course of 25 minutes on a Tecan microplate reader (Männedorf, Switzerland). The fluorescence values were plotted as a function of time and the steepest gradient values were plotted on GraphPad Prism (10.2).

DNA unwinding and translocation

The forked DNA substrate for unwinding was prepared by annealing Cy3-DNA165 with DNA181-BHQ in a 1:1.1 ratio in 1x annealing buffer (20 mM Tris-HCl, 4% glycerol, 0.1 mM EDTA, 40 μ g/mL BSA, 10 mM DTT, 10 mM Mg(OAc)₂ (pH 8)) and incubated at 37 °C overnight. The unwinding reactions contained 1x reaction buffer (20 mM HEPES-KOH, 5 mM Mg(OAc)₂, 50 mM potassium glutamate, 5% glycerol, 0.2 mg/mL BSA, 4 mM DTT, pH 7.5), 100 nM of DnaB and 100 nM of respective CLC protein and incubated on ice for 10 minutes, followed by addition of 50 nM of annealed DNA substrate and incubated further for 10 minutes. The samples were then aliquoted in to a 384-well black microplate (Corning), initiated with 1 mM ATP and 100 nM unlabeled DNA165 (as a trap), and fluorescence (ex 510 nm/ em 580 nm) was read at 30-second intervals over a course of 25 minutes on a Tecan microplate reader (Männedorf, Switzerland). DNA unwinding was monitored through an increase in fluorescence upon release of the BHQ substrate, and the maximal slope was used to calculate the initial velocity (V_0).

The forked DNA substrate for translocation was prepared by mixing Cy3-DNA165, DNA181-BHQ, and DNA180 in 1:5:1 ratio respectively and annealed as mentioned previously. The methodology for translocation was the same as for unwinding with only difference being that 50 nM of annealed DNA translocation fork substrate was added in place of DNA unwinding fork substrate.

Data Availability – All biochemical data presented in this study including, value, gels, images, datasets as well as any strains or plasmids are available upon request to the corresponding author.

Supporting Information - This article contains supporting information.

Acknowledgements – Special thanks to Ben Van Houten (U. Pittsburgh) for providing us with pSCW01, Charles McHenry (U. Colorado) for providing us with initial *E. coli* replisome proteins, plasmids, antibodies, and cell stocks, Mike Cox (U. Wisconsin) for providing the auxotrophic strain, EAW214, and the Superglo GFP

plasmid, pEAW915, and Linda Bloom (U. Florida) for providing the pCOLADuet-1-*dnaX* plasmid. We thank all members of the Trakselis laboratory for productive conversations and insight. We acknowledge the Baylor Molecular Bioscience Center (MBC) and the Center for Microscopy and Imaging (CMI) for providing instrumentation and resources aiding this project.

Author contributions - MUW: conceptualization, formal analysis, investigation, validation, visualization, data curation, methodology, writing—original draft, writing—review and editing; LJB: investigation and formal analysis; MSB: conceptualization and investigation; MAT: conceptualization, formal analysis, investigation, visualization, methodology, supervision, funding acquisition, project administration, resources, writing—original draft, writing— review and editing

Funding and additional information - Research reported in this publication was funded by the NSF MCB (NSF 2105167 to M.A.T.) and supported by Baylor University.

Conflict of interest - The authors declare that they have no conflicts of interest with the contents of this article.

Figure Legends

Figure 1. Schematic of the structure of τ -subunit of the clamp loader complex (CLC) interacting within the bacterial replisome. A) X-ray crystal structures of DnaB (PDBID: 2R6A, *red*), DnaG (PDBID: 1EQN, *orange*), Pol III- β - τ (PDBID: 5FKV, α , ϵ , θ , *green*; β , *cyan*; τ , *orange*), and γ -CLC (PDBID: 3GLI, Domains I, *light steel blue*, II, *Bermuda grey*, III, *akaroa*) were used to model a proposed leading strand bacterial replisome that physically couples unwinding and synthesis. Unstructured Doman IV of τ is shown as dashed line (*mustard*). B) Linear Domain structure (I-V) of τ , highlighting the γ -truncation (431X, *red*), mutations (S617P, *pink*; L635P/D636G, *teal*), and the truncation at 618X (*orange*). The secondary structure sheet (*pink*) and coil (*yellow*) are indicated below based on the available structure and PSIPRED algorithm. C) A closeup of the proposed coupling interaction of Domain V of τ interacting with a hydrophobic surface representation of α is highlighted with a modelled extension of residues 523-536 based on the predicted secondary structure (*yellow hashed*). D) Qualitative assessment of the extent of interaction between His tagged- α subunit of Pol III and respective τ_3 -CLC proteins from a pull-down assay (Fig. S1).

Figure 2. *dnaX:mut* strains show reduced growth rates and fitness. A) Growth curve of *dnaX* strains (*WT* - ● grey, S617P - ■ lavender, L635P/D636G - ▲ teal) at 37 °C monitored using absorbance at OD_{600} . Data plotted is the averaged growth profiles for 10 technical replicates. B) The absolute growth rates (k_2) were calculated from Eqs. 1-2, and the average was plotted as a bar. C) A colorimetric competition assay in which EAW214 ($\Delta arnBAD$) and each of the *dnaX* strains were mixed and allowed to compete for growth. The arabinose present in the plates reduces the dye triphenyl tetrazolium chloride, giving a red color for EAW214 (Ara^-), while the other *dnaX* strains colonies appear white in color (Ara^+) with representative plates shown for each. D) The changes in population of mixed cultures were plotted as a function of time for a minimum of three biological replicates with error bars indicating SE and fit to an exponential decay. E) The selection rates for each of the cultures were calculated using Eq. 3 and plotted. Black bars indicate statistically significant differences with *P*-values indicated and represented by *** <0.001 and **** <0.0001 from an unpaired two-sided *t*-test.

Figure 3. Cell filamentation and chromosome complexity is increased in *dnaX:mut* strains. A) Exponential or B) stationary phase cells stained with DAPI are imaged using an epifluorescence microscope. C) Cell lengths from exponential populations were measured ($n > 80$) and median values were plotted. The error bars denote 95% confidence limits, and black bars indicate the statistically significant differences from *P*-values of **** <0.0001 . D) The singlet and elongated gate populations from FACS are plotted from three biological replicates. Black bars indicate statistically significant differences with *P*-values indicated and represented by ** <0.01 from an unpaired two-sided *t*-test. E) Chromosome complexity observed in *dnaX:mut* strains treated with rifampicin and cephalexin were runout, stained with Sytox Green, and then analyzed using FACS ($n = 10,000$ events). The fluorescence intensity versus counts were plotted as histograms. A temperature sensitive *dnaA:(ts)* strain was used to define the location of cells with single chromosomes along with four or eight chromosomes in the parental cells and are indicated at the top of the graph.

Figure 4. *dnaX:mut* strains induce SOS and increased mutagenesis. A) The growth (OD_{600}) and fluorescence (ex 474 nm / em 509 nm) from induction of sgGFP was monitored for *dnaX:mut* strains in Miller LB media using a plate reader allowing the calculation of specific fluorescence (bottom panel) using Eq. 4. B) Strains were plated on \pm rifampicin (rif) Miller LB plates and cfu were quantified. Mutagenesis frequency for each of the strains were calculated using Eq. 5. The average number of mutants per 10^6 cfu were plotted with the SE indicated. Black bars indicate statistically significant differences where *P*-values are indicated and represented by ** <0.01 or *** <0.001 , from a Mann-Whitney *U*-test. Stationary phase populations of strains expressing sgGFP were examined by C) microscopy or D) FACS ($n = 5000$ events, each for three biological replicates) and E) quantified for ungated %GFP positive cells. F) The average GFP fluorescence intensity per cell measured by FACS was also plotted for gated singlets or elongated cells with the SE indicated. Black bars indicate statistically significant differences, where *P*-values are indicated and represented by * <0.05 , ** <0.01 , or **** <0.0001 , from an unpaired two-sided *t*-test.

Figure 5. Increased ssDNA gaps are present in elongated *dnaX:mut* cells. A) Exponential phase cells were treated with Klenow polymerase and BrdU *in situ*, probed for BrdU in a PLUG assay, and imaged using immunofluorescence microscopy. Blue – DAPI panel represents DNA staining and Pink – BrdU represents ssDNA gaps. The fluorescence intensity of the cells for BrdU positive were also quantified using FACS (n = 10 000 events, each for three biological replicates) and the histograms for gated cells are shown B) for singlets C) elongated cells. Quantification of the %BrdU positive PLUG cells for the D) ungated population or E) comparing singlets and elongated cells are plotted with the SE indicated. Black bars indicate statistically significant differences, where P-values are indicated and represented by * <0.05 or ** <0.01 from an unpaired two-sided *t*-test.

Figure 6. Increased cell death in *dnaX:mut* strains. A) *dnaX:mut* strains grown in Miller LB from a late exponential population were stained for SYTO9 (all cells) and PI (dead cells) and imaged by epifluorescence microscopy. The same populations were analyzed by FACS (n = 5000 events, each for three biological replicates) and the percentage of dead cells (stained with propidium iodide) from the B) ungated population and C) the gated singlet and elongated subpopulations was quantified and plotted. Error bars represent the SE and are contained within the symbol if not visible. Black bars indicate statistically significant differences where P-values are indicated and represented by * <0.05 and ** <0.001 from an unpaired two-sided *t*-test.

Figure 7. DnaB unwinding activity is stimulated by presence of τ -CLC *in vitro*. A) A Cy3-BHQ forked DNA substrate with a 5' overhang for DnaB helicase loading is unwound upon addition of ATP by B) monitoring the averaged Cy3 signal over time. C) The maximal rate (V_0) of the fluorescence increase were plotted (n = 8) for the respective CLC proteins. D) A duplex translocation assay where a 20-base pair duplex was added to the 5' arm and unwinding is monitored by a sensitization of the Cy3 signal over time (n = 4) for E) DnaB only (○ black), + τ_3 -CLC (● grey) and γ_3 -CLC (◆ red) or F) DnaB plus S617P (■ lavender), I618X (▼ yellow), or L635P/D636G (▲ teal). Error bars represent the SD.

Figure 8. Only deletion of the extreme C-terminus of τ disrupts replisome coupling *in vitro*. A) An *E. coli* replisome was reconstituted *in vitro* on a tailed form II DNA substrate and B) the nascent leading strand synthesized products at different timepoints were visualized on a 0.5% alkaline agarose gel using SYBR Gold. C) The average intensity of the total product was plotted against time (n = 3 technical replicates). (WT - ○ grey, Gamma - CLC - ◆ red, S617P - ■ lavender, I618X – ▼ yellow, L635P/D636G - ▲ teal). D) A bar graph depicts the average rate of total product synthesized in the presence of the respective CLCs with error bars representing SE.

References

1. Lewis, J. S., Jergic, S., and Dixon, N. E. (2016) The *E. coli* DNA replication fork. *Enzymes* **39**, 31-88
2. Baker, T. A., Funnell, B. E., and Kornberg, A. (1987) Helicase action of dnaB protein during replication from the *Escherichia coli* chromosomal origin *in vitro*. *J. Biol. Chem.* **262**, 6877-6885
3. Kelman, Z., and O'Donnell, M. (1995) DNA polymerase III holoenzyme: Structure and function of a chromosomal replicating machine. *Annu. Rev. Biochem.* **64**, 171-200
4. Leu, F. P., Georgescu, R., and O'Donnell, M. (2003) Mechanism of the *E. coli* tau processivity switch during lagging-strand synthesis. *Mol. Cell* **11**, 315-327
5. Kim, S., Dallmann, H. G., McHenry, C. S., and Marians, K. J. (1996) Coupling of a replicative polymerase and helicase: A tau-DnaB interaction mediates rapid replication fork movement. *Cell* **84**, 643-650
6. Beattie, T. R., Kapadia, N., Nicolas, E., Uphoff, S., Wollman, A. J., Leake, M. C. *et al.* (2017) Frequent exchange of the DNA polymerase during bacterial chromosome replication. *Elife* **6**, e21763
7. Lewis, J. S., Spinkelink, L. M., Jergic, S., Wood, E. A., Monachino, E., Horan, N. P. *et al.* (2017) Single-molecule visualization of fast polymerase turnover in the bacterial replisome. *Elife* **6**, e23932
8. Kath, J. E., Jergic, S., Heltzel, J. M., Jacob, D. T., Dixon, N. E., Sutton, M. D. *et al.* (2014) Polymerase exchange on single DNA molecules reveals processivity clamp control of translesion synthesis. *Proc. Natl. Acad. Sci. U. S. A.* **111**, 7647-7652
9. Graham, J. E., Marians, K. J., and Kowalczykowski, S. C. (2017) Independent and stochastic action of DNA polymerases in the replisome. *Cell* **169**, 1201-1213 e1217
10. Lewis, J. S., van Oijen, A. M., and Spinkelink, L. M. (2023) Embracing heterogeneity: Challenging the paradigm of replisomes as deterministic machines. *Chem. Rev.* **123**, 13419-13440
11. Gao, D., and McHenry, C. S. (2001) Tau binds and organizes *Escherichia coli* replication proteins through distinct domains. Domain IV, located within the unique C terminus of tau, binds the replication fork, helicase, DnaB. *J. Biol. Chem.* **276**, 4441-4446
12. Tsuchihashi, Z., and Kornberg, A. (1990) Translational frameshifting generates the gamma subunit of DNA polymerase III holoenzyme. *Proc. Natl. Acad. Sci. U. S. A.* **87**, 2516-2520
13. Flower, A. M., and McHenry, C. S. (1990) The gamma subunit of DNA polymerase III holoenzyme of *Escherichia coli* is produced by ribosomal frameshifting. *Proc. Natl. Acad. Sci. U. S. A.* **87**, 3713-3717
14. Gao, D., and McHenry, C. S. (2001) Tau binds and organizes *Escherichia coli* replication through distinct domains. Partial proteolysis of terminally tagged tau to determine candidate domains and to assign domain V as the alpha binding domain. *J. Biol. Chem.* **276**, 4433-4440
15. Jergic, S., Ozawa, K., Williams, N. K., Su, X. C., Scott, D. D., Hamdan, S. M. *et al.* (2007) The unstructured C-terminus of the tau subunit of *Escherichia coli* DNA polymerase III holoenzyme is the site of interaction with the alpha subunit. *Nucleic Acids Res.* **35**, 2813-2824
16. Su, X. C., Jergic, S., Keniry, M. A., Dixon, N. E., and Otting, G. (2007) Solution structure of Domains IVa and V of the tau subunit of *Escherichia coli* DNA polymerase III and interaction with the alpha subunit. *Nucleic Acids Res.* **35**, 2825-2832
17. Dohrmann, P. R., Correa, R., Frisch, R. L., Rosenberg, S. M., and McHenry, C. S. (2016) The DNA polymerase III holoenzyme contains gamma and is not a trimeric polymerase. *Nucleic Acids Res.* **44**, 1285-1297
18. Dallmann, H. G., and McHenry, C. S. (1995) DnaX complex of *Escherichia coli* DNA polymerase III holoenzyme. Physical characterization of the DnaX subunits and complexes. *J. Biol. Chem.* **270**, 29563-29569
19. Pritchard, A. E., Dallmann, H. G., Glover, B. P., and McHenry, C. S. (2000) A novel assembly mechanism for the DNA polymerase III holoenzyme DnaX complex: association of delta' with DnaX(4) forms DnaX(3)delta'. *EMBO J.* **19**, 6536-6545
20. Pritchard, A. E., and McHenry, C. S. (2001) Assembly of DNA polymerase III holoenzyme: co-assembly of gamma and tau is inhibited by DnaX complex accessory proteins but stimulated by DNA polymerase III core. *J Biol Chem* **276**, 35217-35222

21. Hawker, J. R., Jr., and McHenry, C. S. (1987) Monoclonal antibodies specific for the tau subunit of the DNA polymerase III holoenzyme of *Escherichia coli*. Use to demonstrate that tau is the product of the *dnaZ* gene and that both it and gamma, the *dnaZ* gene product, are integral components of the same enzyme assembly. *J. Biol. Chem.* **262**, 12722-12727
22. Chandler, M., Bird, R. E., and Caro, L. (1975) The replication time of the *Escherichia coli* K12 chromosome as a function of cell doubling time. *J. Mol. Biol.* **94**, 127-132
23. Behrmann, M. S., Perera, H. M., Welikala, M. U., Matthews, J. E., Butterworth, L. J., and Trakselis, M. A. (2024) Dysregulated DnaB unwinding induces replisome decoupling and daughter strand gaps that are countered by RecA polymerization. *Under Review*
24. Marians, K. J. (2018) Lesion bypass and the reactivation of stalled replication forks. *Annu. Rev. Biochem.* **87**, 217-238
25. Myka, K. K., and Marians, K. J. (2020) Two components of DNA replication-dependent LexA cleavage. *J. Biol. Chem.* **295**, 10368-10379
26. Sassanfar, M., and Roberts, J. W. (1990) Nature of the SOS-inducing signal in *Escherichia coli*. The involvement of DNA replication. *J. Mol. Biol.* **212**, 79-96
27. Behrmann, M. S., Perera, H. M., Hoang, J. M., Venkat, T. A., Visser, B. J., Bates, D. et al. (2021) Targeted chromosomal *Escherichia coli*:*dnaB* exterior surface residues regulate DNA helicase behavior to maintain genomic stability and organismal fitness. *PLoS genetics* **17**, e1009886
28. Kim, T., Chitteni-Pattu, S., Cox, B. L., Wood, E. A., Sandler, S. J., and Cox, M. M. (2015) Directed evolution of RecA variants with enhanced capacity for conjugational recombination. *PLoS genetics* **11**, e1005278
29. Skarstad, K., Boye, E., and Steen, H. B. (1986) Timing of initiation of chromosome replication in individual *Escherichia coli* cells. *EMBO J.* **5**, 1711-1717
30. Ferullo, D. J., Cooper, D. L., Moore, H. R., and Lovett, S. T. (2009) Cell cycle synchronization of *Escherichia coli* using the stringent response, with fluorescence labeling assays for DNA content and replication. *Methods* **48**, 8-13
31. Hill, T. M., Sharma, B., Valjavec-Gratian, M., and Smith, J. (1997) sfi-independent filamentation in *Escherichia coli* is lexA dependent and requires DNA damage for induction. *J. Bacteriol.* **179**, 1931-1939
32. Chen, S. H., Byrne, R. T., Wood, E. A., and Cox, M. M. (2015) *Escherichia coli* *radD* (*yejH*) gene: A novel function involved in radiation resistance and double-strand break repair. *Mol. Microbiol.* **95**, 754-768
33. Jin, D. J., and Gross, C. A. (1988) Mapping and sequencing of mutations in the *Escherichia coli* *rpoB* gene that lead to rifampicin resistance. *J. Mol. Biol.* **202**, 45-58
34. Sutton, M. D. (2004) The *Escherichia coli* *dnaN159* mutant displays altered DNA polymerase usage and chronic SOS induction. *J. Bacteriol.* **186**, 6738-6748
35. Behrmann, M. S., and Trakselis, M. A. (2022) *In vivo* fluorescent TUNEL detection of single stranded DNA gaps and breaks induced by *dnaB* helicase mutants in *Escherichia coli*. *Methods Enzymol.* **672**, 125-142
36. Paschall, C. O., Thompson, J. A., Marzahn, M. R., Chiraniya, A., Hayner, J. N., O'Donnell, M. et al. (2011) The *E. coli* clamp loader can actively pry open the beta-sliding clamp. *J. Biol. Chem.*
37. Bertram, J. G., Bloom, L. B., Hingorani, M. M., Beechem, J. M., O'Donnell, M., and Goodman, M. F. (2000) Molecular mechanism and energetics of clamp assembly in *Escherichia coli*. The role of ATP hydrolysis when gamma complex loads beta on DNA. *J. Biol. Chem.* **275**, 28413-28420
38. Monachino, E., Ghodke, H., Spinks, R. R., Hoatson, B. S., Jergic, S., Xu, Z. Q. et al. (2018) Design of DNA rolling-circle templates with controlled fork topology to study mechanisms of DNA replication. *Anal. Biochem.* **557**, 42-45
39. Xu, Z. Q., and Dixon, N. E. (2018) Bacterial replisomes. *Curr. Opin. Struct. Biol.* **53**, 159-168
40. Yuan, Q., Dohrmann, P. R., Sutton, M. D., and McHenry, C. S. (2016) DNA polymerase III, but not polymerase IV, must be bound to a tau-containing DnaX complex to enable exchange into replication forks. *J. Biol. Chem.* **291**, 11727-11735
41. Justice, S. S., Hunstad, D. A., Cegelski, L., and Hultgren, S. J. (2008) Morphological plasticity as a bacterial survival strategy. *Nat. Rev. Microbiol.* **6**, 162-168

42. Huisman, O., D'Ari, R., and Gottesman, S. (1984) Cell-division control in *Escherichia coli*: Specific induction of the SOS function SfiA protein is sufficient to block septation. *Proc. Natl. Acad. Sci. U. S. A.* **81**, 4490-4494

43. Simmons, L. A., Foti, J. J., Cohen, S. E., and Walker, G. C. (2008) The SOS regulatory network. *EcoSal Plus* **3**,

44. Dallmann, H. G., Kim, S., Pritchard, A. E., Marians, K. J., and McHenry, C. S. (2000) Characterization of the unique C terminus of the *Escherichia coli* tau DnaX protein. Monomeric C-tau binds alpha and DnaB AND can partially replace tau in reconstituted replication forks. *J. Biol. Chem.* **275**, 15512-15519

45. Perera, H. M., Behrmann, M. S., Hoang, J. M., Griffin, W. C., and Trakselis, M. A. (2019) Contacts and context that regulate DNA helicase unwinding and replisome progression. *Enzymes* **45**, 183-223

46. Little, J. W. (1983) The SOS regulatory system: Control of its state by the level of RecA protease. *J. Mol. Biol.* **167**, 791-808

47. Tondnevis, F., Weiss, T. M., Matsui, T., Bloom, L. B., and McKenna, R. (2016) Solution structure of an "open" *E. coli* Pol III clamp loader sliding clamp complex. *J. Struct. Biol.* **194**, 272-281

48. Jiang, W., Bikard, D., Cox, D., Zhang, F., and Marraffini, L. A. (2013) RNA-guided editing of bacterial genomes using CRISPR-Cas systems. *Nat. Biotechnol.* **31**, 233-239

49. Li, Y. F., Lin, Z. Q., Huang, C., Zhang, Y., Wang, Z. W., Tang, Y. J. et al. (2015) Metabolic engineering of *Escherichia coli* using CRISPR-Cas9 mediated genome editing. *Metab. Eng.* **31**, 13-21

50. Sutton, M. D., Duzen, J. M., and Maul, R. W. (2005) Mutant forms of the *Escherichia coli* beta sliding clamp that distinguish between its roles in replication and DNA polymerase V-dependent translesion DNA synthesis. *Mol. Microbiol.* **55**, 1751-1766

51. Sutton, M. D., Kim, M., and Walker, G. C. (2001) Genetic and biochemical characterization of a novel *umuD* mutation: Insights into a mechanism for UmuD self-cleavage. *J. Bacteriol.* **183**, 347-357

52. Arias-Palomo, E., O'Shea, V. L., Hood, I. V., and Berger, J. M. (2013) The bacterial DnaC helicase loader is a DnaB ring breaker. *Cell* **153**, 438-448

53. Naufer, M. N., Murison, D. A., Rouzina, I., Beuning, P. J., and Williams, M. C. (2017) Single-molecule mechanochemical characterization of *E. coli* Pol III core catalytic activity. *Protein Sci.* **26**, 1413-1426